A regime view of ENSO flavours through clustering in CMIP6 models

Pradeebane Vaittinada Ayar[1,2], David S. Battisti[3], Camille Li[4], Martin King[4], Mathieu Vrac[2], and Jerry Tjiputra[1]

[1]NORCE Norwegian Research Centre AS, Bjerknes Centre for Climate Research, Bergen, Norway
[2]Laboratoire des Sciences du Climat et de l'Environnement (LSCE-IPSL), CEA/CNRS/UVSQ, Université Paris-Saclay, Centre d'Etudes de Saclay, Orme des Merisiers, 91191 Gif-sur-Yvette, France
[3]Department of Atmospheric Sciences, University of Washington, Seattle, WA
[4]Geophysical Institute, University of Bergen and Bjerknes Centre for Climate Research, Bergen, Norway

Key Points:

- A clustering approach identifies two observed warm and cold ENSO regimes to which simulated regimes are matched and consistently evaluated.
- Over historical period, CMIP6 models well simulate ENSO patterns with discrepancies in terms of frequency, seasonality and persistence.
- Future evolution in terms of frequency, magnitude and variability depends on type of cold or warm ENSO regime.

Corresponding author: Pradeebane Vaittinada Ayar, pradeebane@laposte.net; pradeebane@lsce.ipsl.fr

Abstract

El Niño Southern Oscillation (ENSO) flavours in the tropical Pacific are studied from a regime perspective. Five recurring spatial patterns or *regimes* characterising the diversity of ENSO are established using a clustering approach applied to the HadISST sea surface temperature anomalies (SSTA). Two warm (eastern and central El Niño), two cold (basin wide and central La Niña) and a neutral reference regimes are found. Simulated SSTA by the models from the latest Coupled Model Intercomparison Project (CMIP6) are then matched to these reference regimes. This allows for a consistent assessment of the skill of the models in reproducing the reference regimes over the historical period and the change in these regimes under the high-warming Shared Socio-economic Pathway (SSP5.8.5) scenario. Results over the historical period show that models simulate well the reference regimes with some discrepancies. Models simulate overly strong and broad ENSO patterns and have issues in capturing the correct regime seasonality, persistence and transition between regimes. Some models also have difficulty simulating the frequency of regimes, the eastern El Niño regime in particular. In the future, eastern El Niño and central La Niña regimes are expected to be more frequent accompanied with a less frequent neutral regime. The central Pacific El Niño and La Niña regimes are projected to increase in amplitude and variability. Compared to previous studies, our approach gives a common characterisation across models and observations of the diversity of the warm and cold phases of ENSO at the same time established from observations.

Plain Language Summary

A new definition to characterise the diversity of sea surface temperature spatial patterns or *regimes*, typical of the El Niño Southern Oscillation (ENSO) and common to observation and climate model simulations, is established here. This allows for a consistent assessment of the models' skills in reproducing ENSO patterns in the observations and their change under the high-warming scenario. Two warm (eastern and central El Niño), two cold (basin wide and central La Niña) and a neutral reference regimes are found. Over the observed period, models simulate ENSO spatial patterns quite similar to those obtained from the observations with some discrepancies. Models simulate overly strong and broad ENSO patterns and have issues in capturing the correct regime seasonality, persistence and transition between regimes. In the future, eastern El Niño and central La Niña regimes are expected to be more frequent accompanied with a less frequent neutral regime. The central Pacific El Niño and La Niña regimes are projected to increase in amplitude and variability. The novelty of our approach resides in a common characterisation across models and observations of the diversity of the warm and cold phases of ENSO at the same time established from observations.

1 Introduction

El Niño-Southern Oscillation (ENSO) is the leading mode of interannual climate variability (see, e.g., Rasmusson & Carpenter, 1982; Zhang et al., 1997; X. Chen & Wallace, 2015, and references therein). ENSO is a true mode of the coupled atmosphere-ocean system in the tropical Pacific (see Zebiak and Cane (1987) and the review papers by Neelin et al. (1998) and Battisti et al. (2019) and references therein): without the Southern Oscillation, there would be no warm (El Nino event) or cold (La Nina event) phases of ENSO, and vice versa. Owing to the slow decay rate of the ENSO mode, the state of ENSO is predictable up to a year in advance.

ENSO causes seasonal temperature and precipitation anomalies on a global scale (including the frequency of extreme events such has hurricanes) by way of oceanic and atmospheric teleconnections associated with, respectively, changes in the wind stress acting on the ocean and changes in the location of precipitation in the tropical Pacific, (Trenberth

et al., 1998; Davey et al., 2014; X. Chen & Wallace, 2015). As such, ENSO has nearly global impacts on agriculture (e.g., Phillips et al., 1998; Naylor et al., 2001; Iizumi et al., 2014), fisheries (e.g., Bertrand, 2020) and water resources (e.g., Hamlet & Lettenmaier, 1999; Poveda et al., 2001; Nicholas & Battisti, 2008). However, the impact of ENSO on the climate *beyond the tropical Pacific* depends greatly on subtle differences in patterns of sea surface temperature anomalies associated with each ENSO warm and cold event – the so-called different "flavours" of ENSO (K. Takahashi et al., 2011; Thomas et al., 2018; Vimont et al., 2022) – that are a result of the stochastic nature of the atmospheric forcing that provides the energy for ENSO (Vimont et al., 2003). ENSO also alters the global carbon cycle by dominating the year-to-year variability in global atmospheric carbon concentrations (P. J. Rayner et al., 1999). Roughly, land regions emit more CO_2 during El Niño and less CO_2 during La Niña (Betts et al., 2020). In the ocean, ENSO mostly affects the CO_2 fluxes in the tropical Pacific, which is the largest carbon outgassing system to the atmosphere, but with anomaly signal that is the opposite of the land (Feely et al., 2006; T. Takahashi et al., 2009; Vaittinada Ayar et al., 2022).

ENSO events are diverse in terms of the magnitude, duration, and location of sea surface temperature (SST) anomalies (Capotondi et al., 2020). Among the well-known flavours of ENSO are warm (El Niño) events that tend to feature maximum warm anomalies in the far eastern equatorial Pacific and those that tend to have maximum amplitude in the central equatorial Pacific, and cold (La Niña) events that mostly have maximum amplitude in the central equatorial Pacific. That warm events can be more extreme than cold events stems from the non-linear relationship between thermocline displacements and SST anomalies in the eastern Pacific (Battisti et al., 2019).

In order to better consider ENSO diversity, K. Takahashi et al. (2011) introduced an approach that differentiates between central and eastern Pacific warm anomaly patterns in observations or models. It is based on the nonlinear relationship between the two leading empirical orthogonal functions (EOF) of tropical Pacific SST anomalies. K. Takahashi et al. rotated the first and the second principal component (PC1 and PC2) axes by 45° to introduce two indices E and C defined as: $E = \frac{PC1-PC2}{\sqrt{2}}$ and $C = \frac{PC1+PC2}{\sqrt{2}}$. They then showed that E and C represent, respectively, eastern and central Pacific warm events. E and C indices have been extensively used to study warm events in observations and in different generations of numerical climate models (see, Dommenget et al. (2013); K. Takahashi et al. (2011) for the Coupled Model Intercomparison Project Phase 3, CMIP3, Cai et al. (2018); Karamperidou et al. (2017) for CMIP5 and Fredriksen et al. (2020) for CMIP6). This approach allows a better characterisation of warm event diversity (Dommenget et al., 2013) and distinguishes climate models according to their ability to simulate this EOF1/EOF2 non-linearity (Dommenget et al., 2013; Cai et al., 2018).

However, the SST patterns associated with EOF1 and EOF2 (from which PC1 and PC2 are derived to calculate E and C indices) can differ greatly between observations and models and between models (Cai et al., 2018). Indeed, the two model-specific leading EOFs of any given model do not necessarily capture the same SST variability as in observations, making comparisons difficult. Therefore, in order to consistently evaluate the diversity and asymmetry of ENSO events representation across models and observations, a reference framework that provides a common definition of ENSO events based on spatial SST anomaly patterns has to be established.

One approach to characterise modes of variability (for different climate variables) is through regime analysis which has been used to characterise recurrent spatio-temporal structures or regimes (characterising for instance, north Atlantic oscillation seasonal north Atlantic atmospheric circulation or rainfall patterns) , in observations (Vautard, 1990; Yiou & Nogaj, 2004; Cassou, 2008; Vrac & Yiou, 2010; Vrac et al., 2014; Hertig & Jacobeit, 2014) and in climate models (Sanchez-Gomez et al., 2009; Fabiano et al., 2021; Breton et al., 2022). In this paper, a statistical regime analysis of SST anomalies over the tropical Pacific, relying on clustering, is performed to identify recurring spatial pat-

terns (or regimes) of SST typical of ENSO. Their frequency of occurrence, persistence and transitions are studied in observations and CMIP6 models (Eyring et al., 2016) over the historical period (1870-2014). The changes in the regimes under high-warming scenario are also evaluated.

The paper is structured as follows. Section 2.1 details the datasets and pre-processing requirements for the analysis. Section 2.2 explains the methodology. The results regarding the reference observation-based ENSO regimes are presented in Section 3.1. Section 3.2 and 3.3 respectively describe the ability of the models to reproduce reference regimes and their future changes. Conclusions are discussed and summarised in Section 4.

2 Data and Methods

2.1 Data and Preprocessing

The analysis is conducted on monthly sea surface temperature (SST) extracted from the Met Office Hadley Centre HadISST observation-based gridded analyses from 1870 to 2014 (N. A. Rayner et al., 2003) at 1°×1° spatial horizontal resolution and from an ensemble of opportunity of 16 Earth system model (ESM) simulations from the Coupled Model Intercomparison Project 6 (CMIP6, Eyring et al., 2016, see Table 1). In this study, HadISST is considered as the reference observational data-set used to define reference ENSO regimes for evaluating the simulations. All simulations are regridded onto a regular 1°×1° grid using bilinear interpolation provided by climate data operators (CDOs). In this study, analyses are conducted over the HadISST reference period 1870–2014 and the whole ESM simulation period of 1850-2100, combining historical experiment and the high CO_2 Shared Socio-economic Pathway scenario (SSP5-8.5, O'Neill et al., 2016).

Table 1. List of the 16 CMIP6 models used in this study with the horizontal resolution of the ocean component, variant label, model and data references. Note that most of the models have irregular grids and the resolution quoted in the table are approximate.

CMIP6 Model Name	Horizontal Ocean Resolution (lon. by lat. in degree)	Variant Label	ESM Reference	Data
ACCESS-ESM1-5	1°×1°	r1i1p1f1	Law et al. (2017)	Ziehn et al. (2019)
CanESM5	1°×1°	r1i1p2f1	Swart et al. (2019a)	Swart et al. (2019b)
CESM2	1.125°×0.53°	r10i1p1f1	Danabasoglu et al. (2020)	Danabasoglu (2019a)
CESM2-WACCM	1.125°×0.53°	r1i1p1f1	Liu et al. (2019)	Danabasoglu (2019b)
CMCC-ESM2	1°×1°	r1i1p2f1	Lovato et al. (2022)	Lovato et al. (2021)
CNRM-ESM2-1	.3°-1°	r1i1p1f2	Séférian et al. (2019)	Seferian (2018)
GFDL-CM4	0.25°×0.25°	r1i1p1f1	Held et al. (2019)	Guo et al. (2018)
GFDL-ESM4	0.5°×0.5°	r1i1p1f1	Dunne et al. (2020)	Krasting et al. (2018)
IPSL-CM6A-LR	.3°-1°	r1i1p1f1	Boucher et al. (2020)	Boucher et al. (2018)
MIROC-ES2L	1°×1°	r1i1p1f2	Hajima et al. (2020)	Hajima et al. (2019)
MPI-ESM1-2-HR	0.4°×0.4°	r1i1p1f1	Müller et al. (2018)	Jungclaus et al. (2019)
MPI-ESM1-2-LR	1.5°×1.5°	r1i1p1f1	Mauritsen et al. (2019)	Wieners et al. (2019)
MRI-ESM2-0	1°×(0.3-0.5)°	r1i2p1f1	Yukimoto, Kawai, et al. (2019)	Yukimoto, Koshiro, et al. (2019)
NorESM2-LM	1°×1°	r1i1p1f1	Tjiputra et al. (2020)	Seland et al. (2019)
NorESM2-MM	1°×1°	r1i1p1f1	Seland et al. (2020)	Bentsen et al. (2019)
UKESM1-0-LL	1°×1°	r1i1p1f2	Sellar et al. (2019)	Tang et al. (2019)

ENSO regimes are usually defined using SST anomalies (SSTA) over the tropical Pacific. In our study, anomalies are computed over the Pacific domain between 20°S-20°N and from 140°E to the west coast of the Americas from the regridded data (see Figure 2 for the exact study area).

Monthly SSTA at each grid-point are computed by separately removing the trend of each calendar month time-series using a cubic smoothing spline (implemented by the function smooth.spline in R software; R Core Team, 2020) over the period 1870-2014 for HadISST and 1850-2100 for the model simulations. For instance, the non-linear trend of Januaries at a given grid-point is removed from the respective time-series comprising

all January values. The degrees of freedom of the spline is set to 5 for a good compromise between the smoothness (smoothing parameter above 0.8) and the number of parameters (knots) of the spline used to estimate the trend for all tropical Pacific grid-points (Chap.10, Hastie & Tibshirani, 1990).

The Niño 3.4 index is also computed for HadISST and for each model. It corresponds to the standardised area-weighted mean SST anomalies over the Niño 3.4 region: 5°S-5°N × 190°-240°E. These anomalies are computed relative to the 1981-2010 climatology. For the CMIP6 models, the SST values are first detrended over the 1850-2100 period using a cubic spline. Then, the Niño 3.4 index for each model is computed relative to the respective 1981-2010 climatology.

A principal component analysis (PCA) is applied to the reference SSTA fields from HadISST in order to reduce the dimension of the data while keeping most of the variability. SSTA data are weighted by the square root of the cosine of the latitude to give equivalent weights to all grid-cells (Vrac et al., 2014). The first empirical orthogonal function (EOF) accounts for more than 61% of the total SSTA variance while 11 are needed to retain 90%. In this study, the four leading EOFs containing more than 80% of the total variance have been kept for clustering. This choice has been made based on the stability of the clustering performed on these four PCs, and further presented below.

This 4-dimensional (4-d) space defined from the four leading EOFs of HadISST SSTA (sometimes referred to as the "phase space") will be used for the HadISST and the ESM simulations. All monthly anomalies are projected onto these four EOFs to obtain the four leading principal components (PCs) for HadISST and four called "pseudo-PCs" (since these are not the actual PCs) for each ESM. Using the same phase space for all models allows for a consistent comparison of the regime patterns. Indeed, performing a PCA for each model simulation produces model-specific EOFs and constitutes an additional factor to take into account in the analysis. For instance, in some cases information contained in the 4th EOF in HadISST can be contained in the 5th EOF of the model which would penalize the model in terms of performance.

2.2 ENSO Regimes Definition

Our approach consists of clustering the 4-d time series of PCs, x_m, representing monthly HadISST SSTA in the phase space to define the observation-based reference ENSO regimes that are used as benchmark regimes to evaluate the models. The time series of x_m is divided into several groups based on the assumption that the probability density function (pdf) of the x_m can be approximated by a weighted sum of K Gaussian pdfs f_k $(k = 1, \cdots, K)$ also called Gaussian mixture model (GMM; Pearson (1894); Peel and McLachlan (2000)). Each one of these K Gaussians characterises one cluster (or regime) C_k. Thus the multivariate pdf f of x_m fitted to our data is given by:

$$f\,(\,x\,) = \sum_{k\,=\,1}^{K} \pi_k\, f_k(\,x\,;\,\alpha_k\,), \tag{1}$$

where α_k corresponds to the parameters (means μ_k and covariance matrix Ω_k) of f_k and π_k is the mixture ratio also referred to as the prior probability that x_m belongs to C_k. The parameters α_k and π_k of the GMM are to be estimated. The estimation of μ_k, Ω_k and π_k is performed iteratively using the Expectation Maximization (EM, Dempster et al., 1977) algorithm by maximizing the likelihood (Fraley & Raftery, 2002). GMM parameters are initialized by the result of a hierarchical model-based agglomerative clustering. Thus, local maxima are avoided when optimising the likelihood function (e.g. Scrucca and Raftery (2015)). EM is based on the principle that the π_k is calculated when knowing α_k and vice-versa, thus optimizing both. To be more specific, after the initialization:

1. the Expectation-step (or E-step) estimates the posterior probability τ_k^i (update of π_k^i) that the x_m belongs to cluster C_k described by distribution f_k with the current parameter estimates of α_k (at iteration i):

$$\tau_k^i(x_m) = \frac{\pi_k^i \, f_k\,(\,x_m\,,\,\alpha_k^i\,)}{\sum_{k=1}^{K} \pi_k^i \, f_k\,(\,x_m\,,\,\alpha_k^i\,)}. \tag{2}$$

2. Then, the Maximization-step (or M-step) uses the posterior probabilities to improve the estimates of GMM parameters (iteration $i+1$):

$$\pi_k^{i+1} = \frac{1}{n} \sum_{m=1}^{n} \tau_k^i(x_m), \tag{3}$$

$$\mu_k^{i+1} = \frac{1}{n\,\pi_k^{i+1}} \sum_{m=1}^{n} x_m \, \tau_k^i(x_m), \tag{4}$$

$$\Omega_k^{i+1} = \frac{1}{n\,\pi_k^{i+1}} \sum_{m=1}^{n} \tau_k^i(x_m)\,(\,x_m - \mu_k^{i+1}\,)'\,(\,x_m - \mu_k^{i+1}\,), \tag{5}$$

where n is the number of grid-points. The algorithm repeats the E- and M-steps iteratively until the maximum likelihood is reached (convergence of the log-likelihood function) or after a maximum number of iterations.

Finally, each cluster C_k of x_m is defined based on the Gaussian pdfs, according to the principle of posterior maximum:

$$C_k = \{\, x_m \,;\, \pi_k \, f_k\,(\,x_m\,;\,\alpha_k\,) \geq \pi_j \, f_j\,(\,x_m\,;\,\alpha_j\,)\,,\ \forall\, j = 1, \ldots K\}. \tag{6}$$

In other words, a cluster contains every month whose probability of belonging to that cluster is maximised. The freedom of EM in the definition of the regimes depends on the number K of clusters and on the constraints applied to the covariance matrices (Ω_k). K is determined by applying the Bayesian Information Criterion (BIC; Schwarz, 1978). The BIC is used for model selection and helps to prevent overfitting by introducing penalty terms for the complexity of the GMM (*i.e.*, the number of parameters). In our case, minimizing the BIC achieves a good compromise between keeping the model simple and a good representation of the data. The BIC is given by:

$$BIC\,(\,K\,) = p\ log\,(\,n\,) - 2\ log\,(\,L\,), \tag{7}$$

where K is the number of clusters, L the likelihood of the parameterized mixture model, p the number of parameters of the GMM to estimate, and n the size of the sample (*i.e.,* total number of months from January 1870 to December 2014, which is 1740 months).

The clustering described above is performed using the R package 'Mclust' (Scrucca & Raftery, 2015).

A different approach is used to assign each month in the model data to a specific regime. The EM algorithm is not applied, but 4-d representation of monthly SSTA (pseudo-PCs from 1850-2100) of each model is associated with the most appropriate HadISST regime based on the principle of posterior maximum (see Eq. 6). Thus, the regimes are consistently defined for all simulations in the sense that, in the following, ENSO regimes in the models actually represent similar type of ENSO events to those determined from HadISST SSTA. In addition, the variability in the clustering itself as a possible source of noise is ruled out. Such defined regimes are used to compare the regime patterns and their temporal properties across different model simulations within a common reference framework. In practice, the common reference is ensured by computing τ_k^i from Eq. 2 using the GMM parameters estimated from HadISST (hence the common framework) but using pseudo-PCs from each model.

3 Results

3.1 Reference HadISST ENSO Regimes

The EM algorithm has been run to define the optimal number K of ENSO regimes that best describes SSTA spanned by the four leading PCs. From testing K ranging from 2 to 16, the BIC optimisation provides K = 5 as the best number of ENSO regimes. To test the robustness of the number of regimes selected by the BIC, a bootstrap-like procedure has been implemented. The EM algorithm has been applied 250 times to a sub-sample of the total set containing 75% of the data randomly selected (*i.e.* without replacement) and the BIC has been computed for each K from 2 to 10 for each sub-sample. BIC values are presented as violin plots in Figure 1. It confirms the choice of K = 5 regimes since in the clustering of the 250 sub-samples, K=5 comes out as the optimal number of clusters 61.2% of the time.

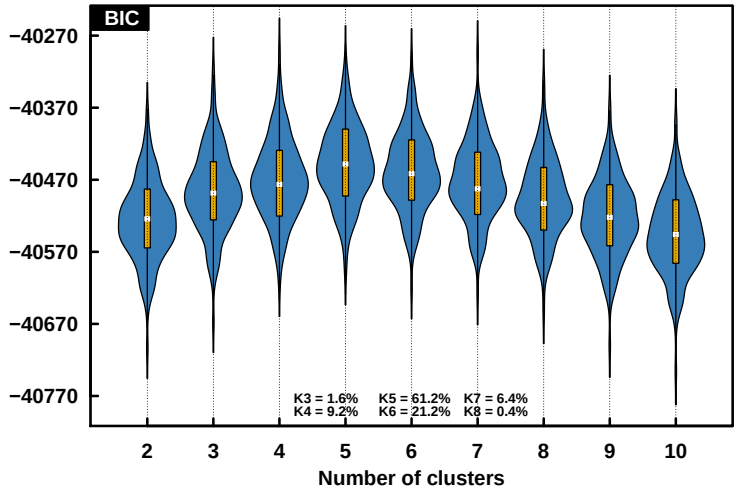

Figure 1. Violin plots represent BIC values as a function of K obtained by applying the EM algorithm 250 times to sub-samples of the total set containing 75% of the data randomly selected. Yellow boxes indicate BIC inter-quartile range and the median is indicated by white dots. The BIC is computed for each K from 2 to 10 for each sub-sample. The ratio (in %) of how often a given value of K is selected as optimal is also given in the bottom.

The sensitivity of the clustering results to the number of PCs has been tested (not shown). Results from the bootstrap-like procedure produce unclear results on the optimal number of clusters and yield a higher optimal number of clusters, some of which are not well liked to known ENSO phases.

Figure 2 a) represents the average HadISST pattern of the five reference regimes determined with the EM algorithm. Two La Niña regimes (basin-wide La Niña BW-LN, central La Niña C-LN), two El Niño regime (central El Niño C-EN, eastern El Niño E-EN) and one Neutral regime are obtained. BW-LN is the most frequent (17.5%) La Niña configuration showing strong negative SSTA covering a large portion of the tropical Pacific. C-LN shows negative anomalies more circumscribed to the equatorial area with positive anomalies in the southeastern part of the domain. Both La Niña regimes have similar ranges of intensity with similar average Niño 3.4 indices (see Fig. 2 b). C-EN is the most frequent El Niño regime with strongest positive SSTA close to the equator. E-EN is the most intense regime with large positive anomalies in the eastern Pacific. Similar results are obtained from the clustering obtained over a shorter period (1950-2014) and from JRA-55 reanalyses over the 1958-2019 period (see supplementary Figure S1; Kobayashi et al. (2015) and Harada et al. (2016)).

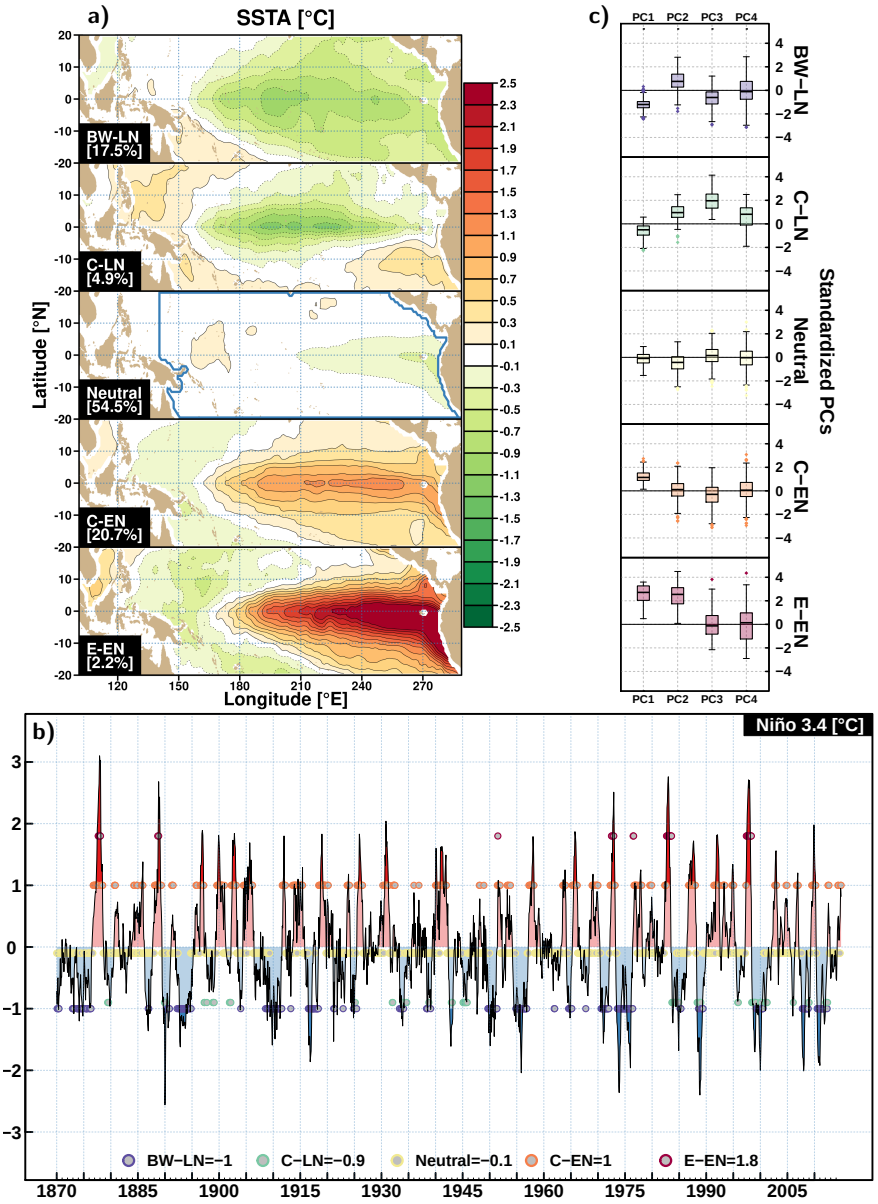

Figure 2. a) Maps of the five ENSO regimes in observations defined by EM. Colours correspond to average SSTA within a regime in °C. The frequency (in %) of occurrence of each regime is given in the bottom left corner of each panel. The blue contour in the Neutral panel indicates the area used to perform the clustering. b) Monthly Niño 3.4 index time series (solid line with red or blue shading when Niño 3.4 is positive or negative). The coloured dots show the assigned regime for each month with the vertical position indicating the average Niño 3.4 value of that cluster (given at the bottom, in °C). c) Boxplots showing the distributions of the four standardised PCs within each regime. Boxes indicate inter-quartile range, whiskers indicate 1.5 times the inter-quartile range from the box and the dots are the values beyond that range and the middle bar the median of the PCs over the 1870-2014 historical period.

The time series of the Niño 3.4 index and the cluster assigned to each month are shown in Fig. 2 b), which depicts that El Niño and La Niña events are well captured by the cluster index. For example, the cluster E-EN corresponds to the strong El Niño events

(*e.g.,* 1877-78,1972-73, 1982-83, 1997-98, K. Takahashi et al., 2011; Ren et al., 2018). Central Pacific El Niño events (1986-87, 1991-92, 1994-1995, 2002-03, 2004-05, and 2009-10) are consistent with cluster C-EN. Similarly, the BW-LN regime contains strong La Niña events (*e.g.,* 1954-56, 1973-74, 1975-76, 1988-89, 1998-2000, 2007-08, Ren et al., 2018, and references therein). C-LN either corresponds to moderate La Niñas, a regime that is in transition from an extreme El Niño (in 1983 and 1998) to an extreme La Niña.

To identify which of the four leading PCs are the most important for each regime, boxplots of the PC distribution for each shown are represented in Fig. 2 c). The warm ENSO patterns are mainly determined by PC1 and PC2 with PC1 dominating for C-EN. Although cold patterns are partly explained by PC1 and PC2, PC3 and PC4 are indispensable for capturing them. In particular, these latter PCs are needed to differentiate BW-LN from the C-LN regimes.

In the next section, consistency in the pseudo-PC weighting across nearly all the models and observations is shown, especially for the two La Niña patterns and the C-EN pattern (see supplementary Figure S2). This indicates that models are able to simulate regime patterns that are similar to those in the observations, and that by projecting model data onto the observed EOFs, temporal information (about *e.g.*, pattern frequencies and probabilities of transition) can be extracted from the models and compared to those in observations. This also advocates for our approach instead of using the dataset specific EOFs.

3.2 Model Evaluation over 1870-2014

ENSO regimes from CMIP6 models are evaluated relative to the reference regimes (HadISST) in terms of spatial patterns, frequency of occurrence of each ENSO regime, the average persistence within each regime (defined as average duration in months a model remains in each regime from the moment that model enters it), and the transition probability from one regime to another.

First, the ability of each model to reproduce the reference patterns is assessed by associating pseudo-PCs from the models with the most appropriate reference regime. Supplementary Figure S3 shows spatial patterns of the ENSO regimes obtained for CMIP6 models and HadISST over the historical period. Interestingly, every model is able to reproduce patterns resembling the reference regimes in terms of spatial distribution and intensity of SSTA. In particular, the asymmetry and the diversity of ENSO event spatial patterns in the reference regimes are well reproduced in the CMIP6 models.

However, there are some notable differences: the extrema in SSTA regimes are usually more intense and spatially broader. (BW-LN, C-EN and E-EN) in the models than in the observations. The extrema of the E-EN regime in the models are not located as far east as in the E-EN regime in HadISST. SSTA patterns are also zonally more extended in the models compared to the patterns in the observations and extend too far west (all except the neutral regime). Figure 3 presents the Taylor diagram for the average SSTA of each ENSO regime in the 1870-2014 historical period. Taylor diagrams are used to evaluate the agreement between average simulated and reference regime patterns. They summarise three statistics comparing simulated grid point 'centred' values ('centred' means that the spatial average is subtracted from to each grid-point value) to a reference value (represented by the red diamonds and lines): 1) the Pearson correlation coefficient measuring the 'similarity' between pairs of centred simulated and reference values is given by the azimuthal position; 2) the centred root mean square error (CRMSE) between the mean centred values of the observations and the simulation is given by the green curves; 3) the standard deviation of simulated and observed pattern values are proportional to the radial distance from the origin (for more details, see Taylor, 2001). Therefore the closer a simulation marker is to the reference one (red diamond), the better is the model.

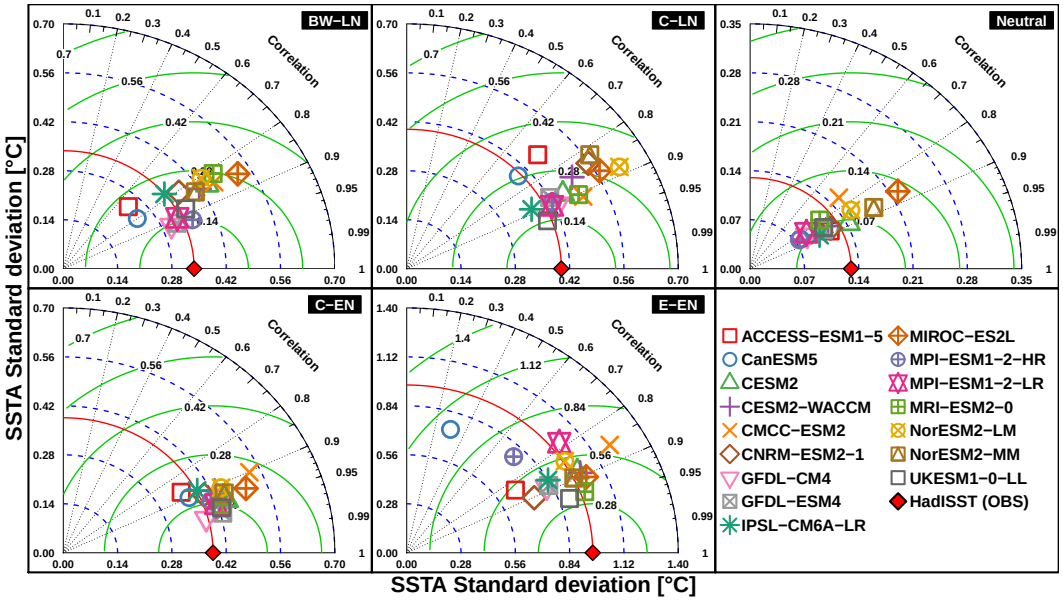

Figure 3. Taylor diagrams for each of the regime patterns from each CMIP6 model and observations (HadISST) over the 1870-2014 period. Each coloured marker refers to one climate model. Red diamonds and red curves indicate the spatial standard deviation of the clusters obtained from the observations.

For each regime, all models show similar spatial patterns as HadISST (spatial correlation typically between 0.8 to 0.9) but with amplitudes that vary greatly across models. Note that the E-EN regime shows greater differences between models and observations, and accordingly, has a larger CRMSE. Models are then ranked based on their statistic performance depicted in the Taylor diagrams. The models are first ranked according each regime and all ranks are then added (the smaller the sum, the better the model) to obtain the rank reported in the first column of Table 2. UKESM1-0-LL, GFDL-CM4, GFDL-ESM4, MPI-ESM1-2-LR and IPSL-CM6A-LR are the top five ESMs for the spatial representation of ENSO.

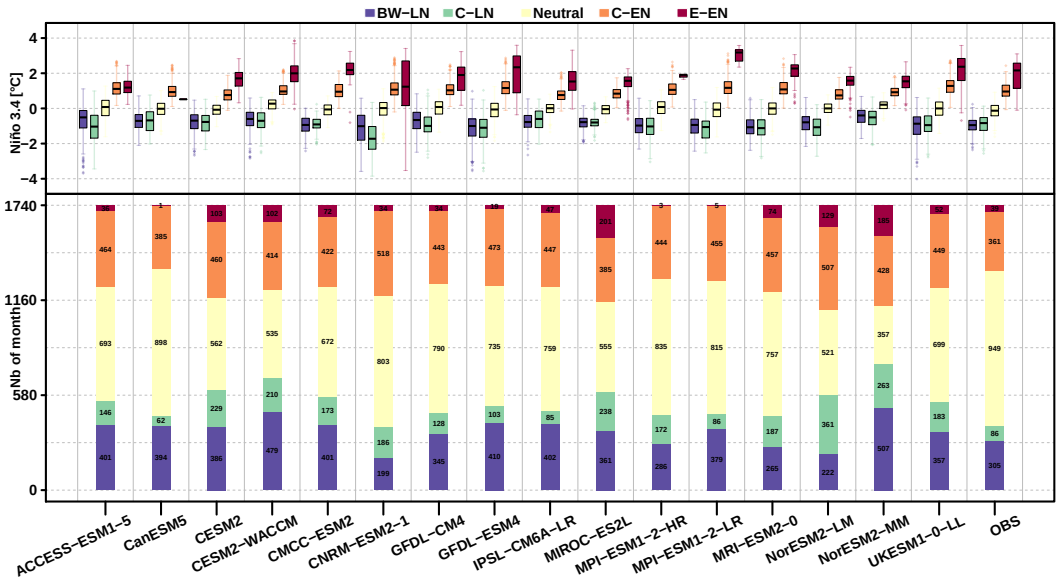

Figure 4. (Bottom) Barplots of each ENSO regime frequency for all the models and HadISST (observations) over the 1870-2014 period. (Top) The boxplots above indicate the Niño 3.4 index distribution for each model and regime.

The frequency of occurrence of each ENSO pattern over the historical period is shown in Figure 4. These vary from one model to another but they roughly agree with the regime frequency in the observations. In particular, the warm E-EN (resp. cold C-LN) regime occurring less frequently than the C-EN (resp. the BW-LN) regimes, is well represented in the models. However, a few models too infrequently simulate the E-EN pattern (CanESM5, and MPI models), or produce too evenly distributed regime frequencies (NorESM2-MM). In order to rank the models, the absolute value of relative frequency bias (in %) is computed for each regime (see supplementary Fig. S4 for actual and absolute bias). Relative frequency biases are larger for C-LN and E-EN, which is expected given their lower occurrence frequency. The frequency bias for each pattern is then combined to produce the "average frequency bias" metric reported in column 2 of Table 2 alongside their corresponding ranks. IPSL-CM6A-LR, GFDL-CM4, MPI-ESM1-2-LR, GFDL-ESM4, and ACCESS-ESM1-5 are the top five ESMs for the frequency representation of ENSO regimes.

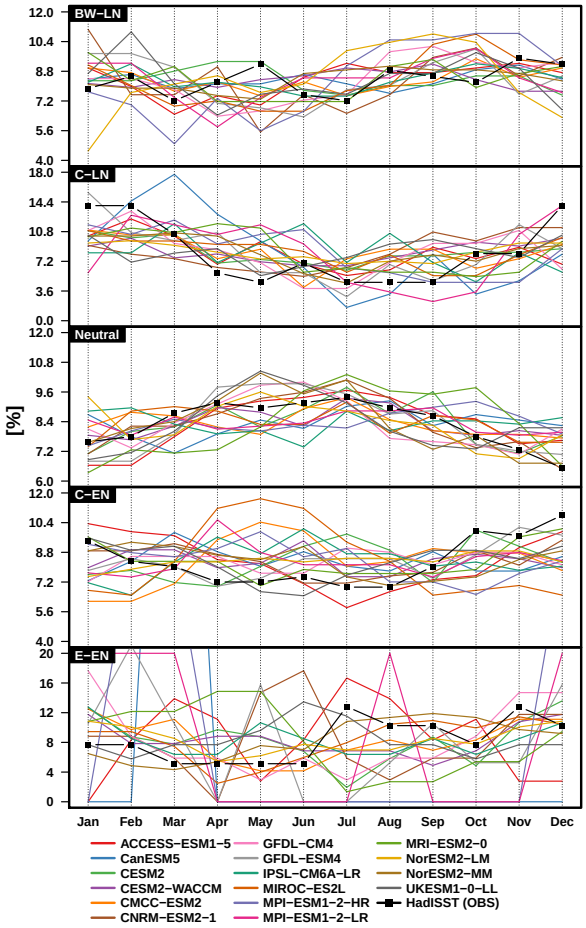

Figure 5. Monthly occurrence ratio (%) for all regimes and all the models and HadISST over the 1870-2014 period.

ENSO events generally peak during boreal winter. Figure 5 depicts the monthly ratio (in %) of how each regime is distributed throughout the year. For the reference regimes, the Neutral pattern occurs more often outside the winter months while C-EN ad C-LN show higher frequencies during the winter. In contrast, BW-LN and E-EN seem to be quite evenly distributed throughout the year. In the models, the seasonality is generally consistent with HadISST for the Neutral regime only. The other regimes do not show

a consistent seasonal cycle in the models. This is consistent with previous studies showing the inability of CMIP6 (and also CMIP3 and CMIP5) models to correctly simulate ENSO peaking in winter (see, H.-C. Chen & Jin, 2021, and references therein). The corresponding Taylor diagram is given in Fig. S5 of the supplementary material. Correlation does not exceed 0.6 for any model meaning that the seasonal variation of pattern occurrences is not well represented in the models. This can be explained by the regime sequences in the models being different from the ones in the reference data-set. Sequences of regime occurrence are evaluated by the average persistence and transitions.

The average persistences of the reference ENSO regimes are 4.3, 3.3, 6.6, 5 and 4.3 months for, respectively the BW-LN, C-LN, Neutral, C-EN and E-EN regimes. Supplementary Fig. S4 gives the persistence bias in the models. Models are in general over-estimating the persistence in the BW-LN (up to 3.5 months) and C-EN regimes (up to 2 months) and under-estimating the persistence in the Neutral regime (up to 2 months). Persistences of E-EN and C-LN regimes, which have lower occurrence frequencies, can be either over- or under-estimated. Consensus between models for these regimes persistence is more difficult to reach given their lower frequency. Similar to the frequency, the absolute persistence bias is computed (see Fig. S4) for each model and the average is reported with their rank in column 2 of Table 2. The top five models are MIROC-ES2L, CMCC-ESM2, MRI-ESM2-0, MPI-ESM1-2-HR and GFDL-CM4.

Figure 6a) shows the month-to-month transition diagram from one reference ENSO regime to another. The probability of remaining in any given regime ranges from 70 to 88%, which is higher than any other transition. The second most favoured transition for BW-LN, C-LN and C-EN is towards the Neutral regime (resp. at 11, 20 and 17%). For the E-EN regime, the second transition is towards C-EN (18%) and there is no direct transition towards the Neutral regime. Direct transitions from either La Niña regime to C-EN and between La Niña regimes are rare. The extreme E-EN sometimes transitions directly to the C-LN regime. Interestingly, this happened after the very strong El Niño events of 1982-83 and 1997-98.

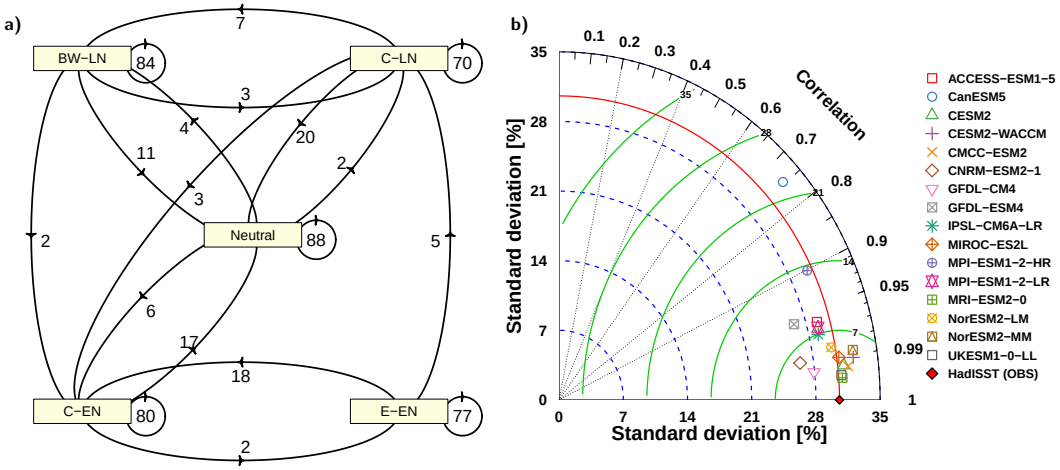

Figure 6. a) Transition diagram from one regime to another obtained for HadISST; values are the transition probability (in %). b) The Taylor diagram evaluating the regime transition probabilities in the CMIP6 models compared to the regime transition probabilities in the observations.

Transition probability matrices for each model and for observations are given in supplementary Figure S6. The Taylor diagram in Fig. 6b compares the ability of the models to reproduce the transitions of the reference regimes. The poorest performing mod-

els tend to underestimate the persistence of E-EN and transition too frequently from E-EN to C-EN (lower right corner of the matrices in Fig. S6), mostly due to the low frequency of occurrence of the E-EN regime. Models are ranked according to their transition behaviour based on the Taylor diagram in column 4 of Table 2. The top five models are MRI-ESM2-0, UKESM1-0-LL, CESM2, CMCC-ESM2 and GFDL-CM4.

Table 2. Model rank for each of four metrics based on model bias (given in parenthesis) or Taylor diagram. The top five models according each metric are bolded. The overall rank is calculated by adding the rank according each metric (given in parenthesis in column 5). The top five models according to the overall rank are highlighted in grey.

	Spatial pattern	Average frequency absolute relative bias (%)	Average persistence absolute bias (month)	Transition probability	Overall rank (total)
ACCESS-ESM1-5	12	**5 (32.9%)**	11 (1.31)	13	12 (41)
CanESM5	13	6 (33.1%)	14 (1.41)	16	16 (49)
CESM2	6	13 (85.0%)	8 (1.13)	**3**	5 (30)
CESM2-WACCM	10	12 (84.2%)	16 (1.78)	7	13 (45)
CMCC-ESM2	16	10 (52.7%)	**2 (0.84)**	**4**	6 (32)
CNRM-ESM2-1	9	8 (44.5%)	7 (1.05)	10	8 (34)
GFDL-CM4	**2**	**2 (22.8%)**	**5 (1.02)**	**5**	1 (14)
GFDL-ESM4	**3**	**4 (31.8%)**	15 (1.45)	14	11 (36)
IPSL-CM6A-LR	**5**	**1 (19.5%)**	12 (1.36)	11	4 (29)
MIROC-ES2L	14	14 (131.7%)	**1 (0.76)**	6	9 (35)
MPI-ESM1-2-HR	7	9 (46.7%)	**4 (0.98)**	15	9 (35)
MPI-ESM1-2-LR	**4**	**3 (30.3%)**	13 (1.37)	12	6 (32)
MRI-ESM2-0	8	11 (53.4%)	**3 (0.85)**	**1**	3 (23)
NorESM2-LM	15	15 (132.7%)	9 (1.17)	9	15 (48)
NorESM2-MM	11	16 (145.5%)	10 (1.31)	8	13(45)
UKESM1-0-LL	**1**	7 (42.8%)	6 (1.03)	**2**	2 (16)

3.3 Future Changes

The changes in the regime frequencies under a high-warming future scenario are analysed. As described in section 2.2, the frequency of the model regimes is obtained by matching the pseudo-PC of each model to the most appropriate reference regime. Thus, changes in regime frequency in the models are not artefacts of potential changes in the spatial patterns of regimes with global warming. Figure 7 shows the ENSO regime frequency over the 1965-2014 historical and 2051-2100 future periods.

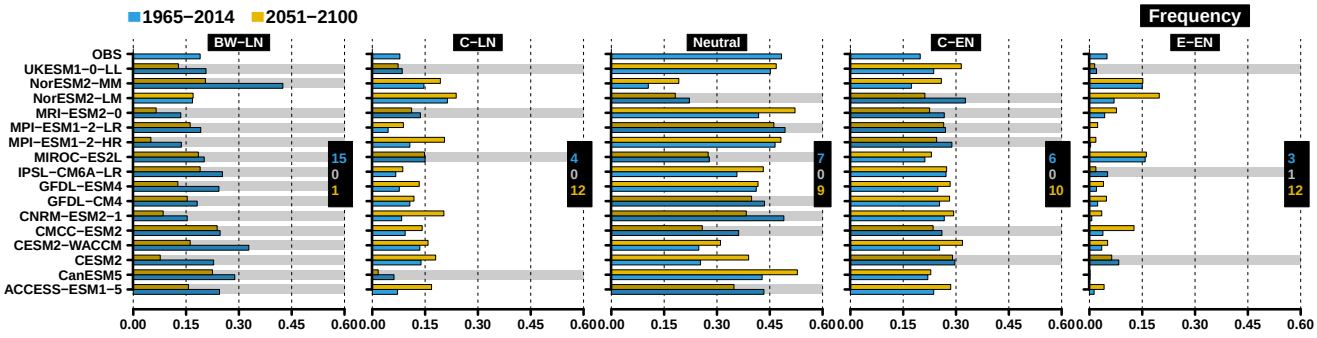

Figure 7. Regime frequencies over the 1965-2014 historical (blue) and the 2051-2100 future (yellow) periods. Grey shading designates the models with lower regime frequency in the future compared to historical period. The number of models with lower, equal and higher occurrence in the future is given in blue, grey and yellow, respectively, for each regime.

The most consistent result is the projected decrease in the BW-LN regime (15 out of 16 models). This decrease is not a mere consequence of the warming since the SSTA

computation has removed the spatial warming trend signals (see section 2.1). In contrast, the other La Niña regime (C-LN) is expected to occur more frequently in the future for 12 out of 16 models. Similarly, E-EN frequency is also expected to increase in the future for the majority (12) of the models. For the C-EN and Neutral regimes, there is no clear consensus, respectively, 10 and 9 models out of 16 projecting increased frequency in the future.

Another way to investigate regime frequency days is through continuous long-term trends in both HadISST and CMIP6 model simulations (respectively over the 1870-2014 and 1850-2100 periods). The linear trends are estimated from the 30-year running mean of the regime frequency time series (see supplementary Figure S7). Figure 8 presents the sign of significant linear trends of ENSO regime frequencies. A trend is considered significant at the 95% confidence level ($\alpha = 0.05$) based on a t-test on the null hypothesis that there is no trend (slope is equal to 0, estimated with *lm* function; R Core Team, 2020). This trend analysis shows that the frequencies of E-EN and C-LN regimes are projected to increase significantly in 13 and 15 models, respectively, by the end of the 21st century. This is consistent with their higher occurrences in the future period shown in Fig. 7 and the historical trends of the reference regimes (Figure S7). The Neutral regime frequencies shows a significant decreasing trend in 11 models and in observations while BW-LN is projected to significantly decrease in only in 50% of the models. Finally, no consensus is reached for C-EN. Same trends are obtained using the non-parametric trend test (*e.g.,* the Theil-Sen test, not shown).

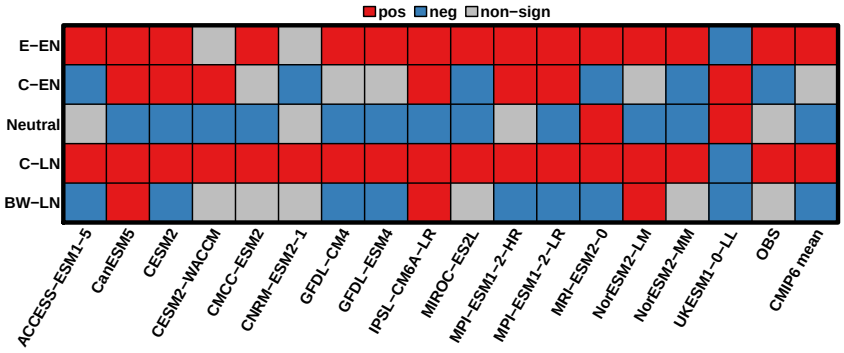

Figure 8. ENSO regime frequency trends over 1850-2100 for CMIP6 models and 1870-2014 of the observations. Significant positive (negative) trends are given in red (blue) and non significant trends are given in grey. The CMIP6 ensemble mean trends are also given.

Figure 9 shows the median and the standard deviation of the Niño 3.4 index, within each cluster, for the reference and model regimes over the 1965-2014 historical and the 2051-2100 future periods. The C-EN and C-LN clusters are associated with more intense SSTA in the future for the 13 models with a larger median Niño 3.4 index. For BW-LN and E-EN, the results are mixed with, respectively, 9 and 8 of the models projecting more intense patterns. In terms of variability, the C-LN, Neutral and C-EN regimes are expected to show increased variability with, respectively, 12, 15 and 15 with higher intra-regime Niño 3.4 standard deviation in the future. Similar to the median, only 9 models project an increase in Niño 3.4 variability for the BW-LN and E-EN regimes.

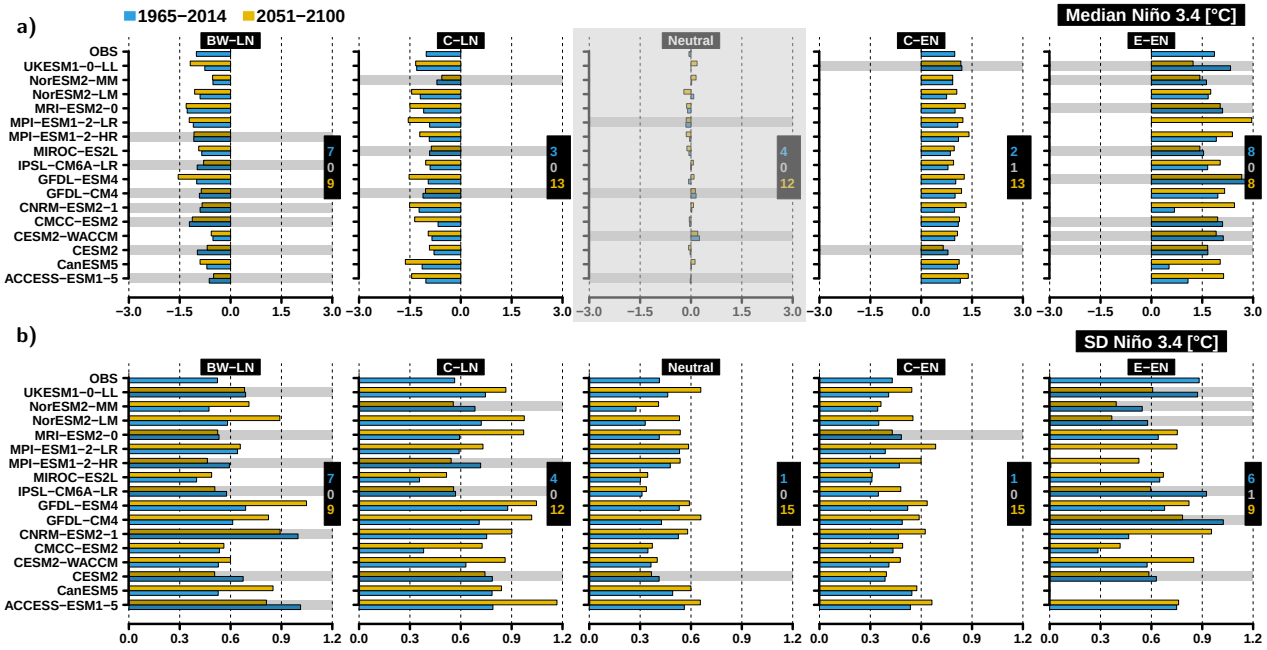

Figure 9. Median a) and standard deviation b) of Niño 3.4 for each regime over the 1965-2014 historical (blue) and the 2051-2100 future (yellow) periods. Grey shading designates the models with smaller median and standard deviation in the future compared to the historical period. The number of models with smaller, equal and larger Niño 3.4 statistics in the future are given in blue, grey and yellow, respectively, for each regime. The Neutral panel is greyed out for the median because it is not meaningful and hence is not considered.

4 Conclusions and Discussions

ENSO diversity is studied using sea surface temperature anomaly data from a HadISST reference dataset and 16 CMIP6 climate models to characterize historical (1870-2014) and future (to the end of 21st century) ENSO patterns. A clustering approach has been used to perform the analysis, allowing new insight into the ENSO diversity.

4.1 Regime Definition

ENSO events are diverse in terms of the magnitude, duration, and location of the SST anomalies (Capotondi et al., 2020; Cai et al., 2021). For example, strong El Niño events with maximum warm anomalies located in the eastern Pacific region are less frequent and more intense (larger SSTA) than strong La Niña which have maximum cold anomalies. Warm anomalies concentrated in the central Pacific tend to be associated with moderate El Niño events. This diversity has been studied using combinations of indices defined by SSTA averaged over specific regimes (*e.g.,* Niño 3.4) and those defined by EOF analysis pf the SSTA (Trenberth & Stepaniak, 2001; Larkin & Harrison, 2005; Ashok et al., 2007; K. Takahashi et al., 2011). Applying such approaches to models is, however, problematic given know biases in their representation of spatial patterns and EOF-partitioning of the tropical Pacific variability (Battisti et al., 2019).

In this study, the GMM-based clustering approach has been used to define ENSO regimes. The more commonly used k-means approach (see, Fabiano et al., 2021, and the references therein) can be seen as a particular case of GMM where each month is assigned

to one (and only one) of the K components and covariance matrices are forced to be diagonal, equal and with very small variances (see section 16.1 of Press et al., 2007, for more details). In GMM, the assignment to the K components is probabilistic (see, Eq. 2 and 6), and there are fewer restrictions on the covariance matrices (see Eq. 5). Our choice of GMM over k-means is motivated by two factors:

1. The number of clusters in GMM is objectively defined by the BIC, hence there is no need for *a priori* knowledge about the clusters themselves.
2. More flexibility in the covariance matrices in the GMM using the EM algorithm allows for very different shape and size of cluster which is required given the diversity of ENSO. These clusters are better able to represent the diversity of ENSO, including extreme or rare events. Using k-means with all equal shaped clusters tends to generate equal size clusters.

Thus, the diversity of ENSO event is well captured by our GMM-based clusters in the observations (see Fig. 2). From this method each monthly SSTA pattern is classified into one of five possible regimes, including two El Niño regimes (a strong Eastern Pacific one, E-EN and a more frequent moderate central Pacific one, C-EN); two La Niña regimes (a more frequent long lasting La Niña covering almost the whole Pacific domain, BW-LN, that includes the strongest La Niña events and a central La Niña, C-LN) and finally a Neutral pattern regrouping light to very tenuous SSTA.

As seen in section 3.1, between warm ENSO patterns, E-EN is mainly determined by PC1 and PC2 while PC1 dominating for C-EN. Although cold patterns are partly explained by PC1 and PC2, PC3 and PC4 are indispensable to determine them, and in particular, to differentiate BW-LN from the C-LN regimes. K. Takahashi et al. (2011) found that warm events that peak in the eastern Pacific are well described by the difference in the first two EOFs (i.e., by PC1*E1 - PC2*E2) while those for central Pacific warm events could be described by the sum of the first EOFs (i.e., PC*E1 + PC2*E2). This is consistent with our result except in our case we found that PC2 does not contribute to discriminate central warm events. One of the added-values of our approach is the use of four EOFs allows a more comprehensive characterisation. In particular, it allows to characterise both warm and cold ENSO regimes and the transitions between them suggesting that the PCs describe evolution rather than different types of events

In addition, this study focuses on retrieving the observed SSTA pattern in the models by matching models data to the reference regimes. Our definition of the model regime allows for a direct comparison between SSTA pattern from the CMIP6 models and those from the HadISST reference data.

4.2 Reference and Modelled Historical ENSO Regimes

ENSO-induced SST anomaly patterns in HadISST over 1870-2014 are quite well represented in the models. However, there are some discrepancies between the observed and simulated regimes:

1. models generally show broader and more intense ENSO patterns that extend further west;
2. a few models too infrequently simulate the extreme E-EN pattern (CanESM5, and MPI models), or produce too evenly distributed regime frequencies (*e.g.* CESM2 and NorEMS2 and MIROC-ES2L models);
3. seasonal distributions of El Niño and La Niña regimes are not well represented in the models;
4. persistence of C-EN and BW-LN regimes are overestimated while the persistence in the Neutral regime is underestimated in the models;

5. overall transitions between the reference and models regimes are similar except for the models with too infrequency E-EN events.

Compared to conventional ENSO indices or the two leading EOFs approach, our four-dimensional (4 EOFs) clusters not only capture essential features of the SSTA spatial patterns along the equator (Central or Eastern) but also the meridional features. These patterns provide valuable information about ENSO evolution, particularly, the zonal and meridional span of the SSTA and the zonal motion along the equator reflecting the intrinsic dynamic processes of ENSO. Our GMM-based clustering approach has the advantage of showing the transitions among regimes of the ENSO associated SSTA pattern as well as its magnitude. The characterisation of ENSO dynamic simulated in CMIP6 models by matching model data to the reference ENSO clusters allows to evaluate the quality of the models in simulating ENSO and their ability to produce the associated SSTA reference patterns. In addition, in previous ENSO studies, only the properties of one phase (El Niño or La Niña) with filtered data (often seasonally) are analysed (see Cai et al., 2021, and the references therein). The method developed in this study allows to study the ENSO in the models continuously without filtering the data (PCA put aside).

This method also may provide some potential for ENSO forecast from SST forecast. In particular, pseudo-PCs can be computed from SSTA forecasts and Eq. 2 can then be used to forecast the most probable ENSO regime that will develop (in particular, the type of El Niño or La Niña).

Last but not least, future studies should further investigate local implications of the different regimes, by defining regimes accounting for local-scale meteorological patterns (e.g., precipitation, wind speed) and large-scale patterns (*e.g.,* Vrac & Yiou, 2010). Understanding the effects of ENSO changes locally is important to anticipate future changes in weather conditions and the consequences for nature and society.

4.3 ENSO Regime Changes in the Future

Under a high warming scenario, the ENSO regimes are expected to change as follows:

1. The more extreme La Niña (BW-LN) regime is in general projected to become less frequent but there is no consensus in terms of changes in magnitude and variability;
2. There is a strong consensus among the models that the central, moderate La Niña (C-LN) regime will become more frequent (significantly), intense and variable;
3. The Neutral regime will become significantly less frequent and more variable in the future;
4. There is no consensus for the moderate El Niño (C-EN) in terms of frequency, but it is projected to become more intense and variable by the majority of the models;
5. Similarly the strong El Nino (E-EN) regime is projected to become significantly more frequent but there is no consensus in terms of changes in magnitude and variability.

Given the diversity of ENSO-related SSTA principal modes of variability in the models (typically located in central or eastern Pacific), the use of model-specific indices (cf. E and C definition in the introduction) has typically been favoured to reach a better agreement among the models regarding the assessment of ENSO changes (*e.g*, Cai et al., 2018). However, using model-specific indices presumes that the simulated spatial ENSO patterns across the different models are similar (i.e., according to those indices) while it is not the case in reality. The methodology developed in this study is able to capture robust trends of the different regimes based on a common definition of SSTA patterns. In

addition to providing information on which types of ENSO events are expected to become more or less likely in the future, the conclusions are more robust compared to previous studies in the sense that eastern or central patterns in the models are actually located in the same circumscribed area in all models. Another advantage of our approach is the ability to analyse changes in the magnitude and variability using well known Niño indices (Niño 3.4 index here) and not only in model-specific variability indices as previously done. In particular, it is possible to study ENSO features within each regime and state how their magnitude and variability will change in the future.

Open Research Section

The HadISST analysis SST product used in this study is accessible from their Web site at `https://www.metoffice.gov.uk/hadobs/hadisst/data/HadISST_sst.nc.gz`. The CMIP6 data used in the analysis were obtained from `https://esgf-node.llnl.gov/search/cmip6`.

Acknowledgments

All computations and figures are made using the R free software (R Core Team, 2020). PV and JT acknowledge funding from the Research Council of Norway (COLUMBIA-275268, CE2COAST-318477, and EASMO-322912).

We acknowledge the World Climate Research Programme, which, through its Working Group on Coupled Modelling, coordinated and promoted CMIP6. We thank the climate modelling groups for producing and making available their model output, the Earth System Grid Federation (ESGF) for archiving the data and providing access, and the multiple funding agencies who support CMIP6 and ESGF.

References

Ashok, K., Behera, S. K., Rao, S. A., Weng, H., & Yamagata, T. (2007). El niño modoki and its possible teleconnection. *Journal of Geophysical Research: Oceans*, *112*(C11). doi: https://doi.org/10.1029/2006JC003798

Battisti, D. S., Vimont, D. J., & Kirtman, B. P. (2019). 100 Years of progress in understanding the dynamics of coupled atmosphere/ocean variability. *Meteorological Monographs*, *59*, 8.1–8.57. doi: 10.1175/AMSMONOGRAPHS-D-18-0025.1

Bentsen, M., Oliviè, D. J. L., Seland, y., Toniazzo, T., Gjermundsen, A., Graff, L. S., ... Schulz, M. (2019). *NCC NorESM2-MM model output prepared for CMIP6 CMIP historical.* Earth System Grid Federation. Retrieved from `https://doi.org/10.22033/ESGF/CMIP6.8040` doi: 10.22033/ESGF/CMIP6.8040

Bertrand, A. (2020). *El Niño Southern Oscillation (ENSO) effects on fisheries and aquaculture* (No. 660).

Betts, R. A., Burton, C. A., Feely, R. A., Collins, M., Jones, C. D., & Wiltshire, A. J. (2020). ENSO and the Carbon Cycle. In (p. 453-470). In El Niño Southern Oscillation in a Changing Climate (eds M.J. McPhaden, A. Santoso and W. Cai). doi: 10.1002/9781119548164.ch20

Boucher, O., Denvil, S., Levavasseur, G., Cozic, A., Caubel, A., Foujols, M.-A., ... Cheruy, F. (2018). *IPSL IPSL-CM6A-LR model output prepared for CMIP6 CMIP historical.* Earth System Grid Federation. Retrieved from `https://doi.org/10.22033/ESGF/CMIP6.5195` doi: 10.22033/ESGF/CMIP6.5195

Boucher, O., Servonnat, J., Albright, A. L., Aumont, O., Balkanski, Y., Bastrikov, V., ... Vuichard, N. (2020). Presentation and Evaluation of the IPSL-CM6A-LR Climate Model. *Journal of Advances in Modeling Earth Systems*, *12*(7), e2019MS002010. doi: 10.1029/2019MS002010

Breton, F., Vrac, M., Yiou, P., Vaittinada Ayar, P., & Jézéquel, A. (2022). Seasonal circulation regimes in the north atlantic: Towards a new seasonality. *International Journal of Climatology*, *42*(11), 5848-5870. doi: https://doi.org/10.1002/joc.7565

Cai, W., Santoso, A., Collins, M., Dewitte, B., Karamperidou, C., Kug, J.-S., ... Zhong, W. (2021). Changing El Niño–Southern Oscillation in a warming climate. *Nature Reviews Earth & Environment*, *2*(9), 628–644. doi: 10.1038/s43017-021-00199-z

Cai, W., Wang, G., Dewitte, B., Wu, L., Santoso, A., Takahashi, K., ... McPhaden, M. J. (2018). Increased variability of eastern Pacific El Niño under greenhouse warming. *Nature*, *564*(7735), 201–206. doi: 10.1038/s41586-018-0776-9

Capotondi, A., Wittenberg, A. T., Kug, J.-S., Takahashi, K., & McPhaden, M. J. (2020). Enso diversity. In (pp. 65–86). In El Niño Southern Oscillation in a Changing Climate (eds M.J. McPhaden, A. Santoso and W. Cai). doi: 10.1002/9781119548164.ch4

Cassou, C. (2008). Intraseasonal interaction between the Madden–Julian Oscillation and the North Atlantic Oscillation. *Nature*, *455*, 523–527. doi: 10.1038/nature07286

Chen, H.-C., & Jin, F.-F. (2021). Simulations of enso phase-locking in cmip5 and cmip6. *Journal of Climate*, *34*(12), 5135 - 5149. doi: 10.1175/JCLI-D-20-0874.1

Chen, X., & Wallace, J. M. (2015). ENSO-like variability: 1900–2013. *Journal of Climate*, *28*(24), 9623–9641. doi: 10.1175/JCLI-D-15-0322.1

Danabasoglu, G. (2019a). *NCAR CESM2 model output prepared for CMIP6 CMIP historical.* Earth System Grid Federation. Retrieved from `https://doi.org/10.22033/ESGF/CMIP6.7627` doi: 10.22033/ESGF/CMIP6.7627

Danabasoglu, G. (2019b). *NCAR CESM2-WACCM model output prepared for CMIP6 CMIP historical.* Earth System Grid Federation. Retrieved from `https://doi.org/10.22033/ESGF/CMIP6.10071` doi: 10.22033/ESGF/CMIP6.10071

Danabasoglu, G., Lamarque, J.-F., Bacmeister, J., Bailey, D. A., DuVivier, A. K., Edwards, J., ... Strand, W. G. (2020). The community earth system model version 2 (cesm2). *Journal of Advances in Modeling Earth Systems*, *12*(2), e2019MS001916. doi: https://doi.org/10.1029/2019MS001916

Davey, M., Brookshaw, A., & Ineson, S. (2014). The probability of the impact of ENSO on precipitation and near-surface temperature. *Climate Risk Management*, *1*, 5–24. doi: 10.1016/j.crm.2013.12.002

Dempster, A. P., Laird, N. M., & Rubin, D. B. (1977). Maximum likelihood from incomplete data via the em algorithm. *Journal of the Royal Statistical Society: Series B (Methodological)*, *39*(1), 1–22. doi: 10.1111/j.2517-6161.1977.tb01600.x

Dommenget, D., Bayr, T., & Frauen, C. (2013). Analysis of the non-linearity in the pattern and time evolution of El Niño southern oscillation. *Climate dynamics*, *40*(11), 2825–2847. doi: 10.1007/s00382-012-1475-0

Dunne, J. P., Horowitz, L. W., Adcroft, A. J., Ginoux, P., Held, I. M., John, J. G., ... Zhao, M. (2020). The GFDL Earth System Model Version 4.1 (GFDL-ESM 4.1): Overall Coupled Model Description and Simulation Characteristics. *Journal of Advances in Modeling Earth Systems*, *12*(11), e2019MS002015. doi: 10.1029/2019MS002015

Eyring, V., Bony, S., Meehl, G. A., Senior, C. A., Stevens, B., Stouffer, R. J., & Taylor, K. E. (2016). Overview of the Coupled Model Intercomparison Project Phase 6 (CMIP6) experimental design and organization. *Geoscientific Model Development*, *9*(5), 1937–1958. doi: 10.5194/gmd-9-1937-2016

Fabiano, F., Meccia, V. L., Davini, P., Ghinassi, P., & Corti, S. (2021). A regime view of future atmospheric circulation changes in northern mid-latitudes.

Weather and Climate Dynamics, *2*(1), 163–180. doi: 10.5194/wcd-2-163-2021

Feely, R. A., Takahashi, T., Wanninkhof, R., McPhaden, M. J., Cosca, C. E., Sutherland, S. C., & Carr, M.-E. (2006). Decadal variability of the air-sea CO_2 fluxes in the equatorial Pacific Ocean. *Journal of Geophysical Research: Oceans*, *111*(C8). doi: 10.1029/2005JC003129

Fraley, C., & Raftery, A. E. (2002). Model-based clustering, discriminant analysis, and density estimation. *Journal of the American statistical Association*, *97*(458), 611–631. doi: 10.1198/016214502760047131

Fredriksen, H.-B., Berner, J., Subramanian, A. C., & Capotondi, A. (2020). How does el niño–southern oscillation change under global warming—a first look at cmip6. *Geophysical Research Letters*, *47*(22), e2020GL090640. doi: https://doi.org/10.1029/2020GL090640

Guo, H., John, J. G., Blanton, C., McHugh, C., Nikonov, S., Radhakrishnan, A., ... Zhang, R. (2018). *NOAA-GFDL GFDL-CM4 model output historical.* Earth System Grid Federation. Retrieved from `https://doi.org/10.22033/ESGF/CMIP6.8594` doi: 10.22033/ESGF/CMIP6.8594

Hajima, T., Abe, M., Arakawa, O., Suzuki, T., Komuro, Y., Ogura, T., ... Tachiiri, K. (2019). *MIROC MIROC-ES2L model output prepared for CMIP6 CMIP historical.* Earth System Grid Federation. Retrieved from `https://doi.org/10.22033/ESGF/CMIP6.5602` doi: 10.22033/ESGF/CMIP6.5602

Hajima, T., Watanabe, M., Yamamoto, A., Tatebe, H., Noguchi, M. A., Abe, M., ... Kawamiya, M. (2020). Development of the MIROC-ES2L Earth system model and the evaluation of biogeochemical processes and feedbacks. *Geoscientific Model Development*, *13*(5), 2197–2244. doi: 10.5194/gmd-13-2197-2020

Hamlet, A. F., & Lettenmaier, D. P. (1999). Columbia River streamflow forecasting based on ENSO and PDO climate signals. *Journal of water resources planning and management*, *125*(6), 333–341. doi: 10.1061/(ASCE)0733-9496(1999)125:6(333)

Harada, Y., Kamahori, H., Kobayashi, C., Endo, H., Kobayashi, S., Ota, Y., ... Takahashi, K. (2016). The JRA-55 Reanalysis: Representation of Atmospheric Circulation and Climate Variability. *Journal of the Meteorological Society of Japan. Ser. II*, *94*(3), 269-302. doi: 10.2151/jmsj.2016-015

Hastie, T., & Tibshirani, R. (1990). *Generalized Additive Models.* Chapman and Hall. Retrieved from `http://books.google.co.uk/books?id=qa29r1Ze1coC`

Held, I. M., Guo, H., Adcroft, A., Dunne, J. P., Horowitz, L. W., Krasting, J., ... Zadeh, N. (2019). Structure and Performance of GFDL's CM4.0 Climate Model. *Journal of Advances in Modeling Earth Systems*, *11*(11), 3691-3727. doi: 10.1029/2019MS001829

Hertig, E., & Jacobeit, J. (2014). Variability of weather regimes in the north atlantic-european area: past and future. *Atmospheric Science Letters*, *15*(4), 314–320. doi: 10.1002/asl2.505

Iizumi, T., Luo, J.-J., Challinor, A. J., Sakurai, G., Yokozawa, M., Sakuma, H., ... Yamagata, T. (2014). Impacts of El Niño - Southern Oscillation on the global yields of major crops. *Nature Communications*, *5*(1), 3712. doi: 10.1038/ncomms4712

Jungclaus, J., Bittner, M., Wieners, K.-H., Wachsmann, F., Schupfner, M., Legutke, S., ... Roeckner, E. (2019). *MPI-M MPI-ESM1.2-HR model output prepared for CMIP6 CMIP historical.* Earth System Grid Federation. Retrieved from `https://doi.org/10.22033/ESGF/CMIP6.6594` doi: 10.22033/ESGF/CMIP6.6594

Karamperidou, C., Jin, F.-F., & Conroy, J. L. (2017). The importance of ENSO nonlinearities in tropical pacific response to external forcing. *Climate Dynamics*, *49*(7), 2695–2704. doi: 10.1007/s00382-016-3475-y

Kobayashi, S., Ota, Y., Harada, Y., Ebita, A., Moriya, M., Onoda, H., ... Takahashi, K. (2015). The JRA-55 Reanalysis: General Specifications and Basic

Characteristics. *Journal of the Meteorological Society of Japan. Ser. II*, *93*(1), 5-48. doi: 10.2151/jmsj.2015-001

Krasting, J. P., John, J. G., Blanton, C., McHugh, C., Nikonov, S., Radhakrishnan, A., ... Zhao, M. (2018). *NOAA-GFDL GFDL-ESM4 model output prepared for CMIP6 CMIP historical.* Earth System Grid Federation. Retrieved from `https://doi.org/10.22033/ESGF/CMIP6.8597` doi: 10.22033/ESGF/CMIP6.8597

Larkin, N. K., & Harrison, D. E. (2005). Global seasonal temperature and precipitation anomalies during el niño autumn and winter. *Geophysical Research Letters*, *32*(16). doi: https://doi.org/10.1029/2005GL022860

Law, R. M., Ziehn, T., Matear, R. J., Lenton, A., Chamberlain, M. A., Stevens, L. E., ... Vohralik, P. F. (2017). The carbon cycle in the Australian Community Climate and Earth System Simulator (ACCESS-ESM1) – Part 1: Model description and pre-industrial simulation. *Geoscientific Model Development*, *10*(7), 2567–2590. doi: 10.5194/gmd-10-2567-2017

Liu, S.-M., Chen, Y.-H., Rao, J., Cao, C., Li, S.-Y., Ma, M.-H., & Wang, Y.-B. (2019). Parallel Comparison of Major Sudden Stratospheric Warming Events in CESM1-WACCM and CESM2-WACCM. *Atmosphere*, *10*(11). doi: 10.3390/atmos10110679

Lovato, T., Peano, D., & Butenschön, M. (2021). *Cmcc cmcc-esm2 model output prepared for cmip6 cmip historical.* Earth System Grid Federation. Retrieved from `https://doi.org/10.22033/ESGF/CMIP6.13195` doi: 10.22033/ESGF/CMIP6.13195

Lovato, T., Peano, D., Butenschön, M., Materia, S., Iovino, D., Scoccimarro, E., ... Navarra, A. (2022). Cmip6 simulations with the cmcc earth system model (cmcc-esm2). *Journal of Advances in Modeling Earth Systems*, *14*(3), e2021MS002814. doi: 10.1029/2021MS002814

Mauritsen, T., Bader, J., Becker, T., Behrens, J., Bittner, M., Brokopf, R., ... Roeckner, E. (2019). Developments in the MPI-M Earth System Model version 1.2 (MPI-ESM1.2) and Its Response to Increasing CO_2. *Journal of Advances in Modeling Earth Systems*, *11*(4), 998-1038. doi: 10.1029/2018MS001400

Müller, W. A., Jungclaus, J. H., Mauritsen, T., Baehr, J., Bittner, M., Budich, R., ... Marotzke, J. (2018). A Higher-resolution Version of the Max Planck Institute Earth System Model (MPI-ESM1.2-HR). *Journal of Advances in Modeling Earth Systems*, *10*(7), 1383-1413. doi: 10.1029/2017MS001217

Naylor, R. L., Falcon, W. P., Rochberg, D., & Wada, N. (2001). Using El Niño/Southern Oscillation climate data to predict rice production in Indonesia. *Climatic Change*, *50*(3), 255–265. doi: 10.1023/A:1010662115348

Neelin, J. D., Battisti, D. S., Hirst, A. C., Jin, F.-F., Wakata, Y., Yamagata, T., & Zebiak, S. E. (1998). ENSO theory. *Journal of Geophysical Research-Oceans*, *103*(C7), 14261-14290. doi: 10.1029/97JC03424\%7D

Nicholas, R. E., & Battisti, D. S. (2008). Drought recurrence and seasonal rainfall prediction in the Rio Yaqui Basin, Mexico. *Journal of Applied Meteorology and Climatology*, *47*(4), 991–1005. doi: 10.1175/2007JAMC1575.1

O'Neill, B. C., Tebaldi, C., van Vuuren, D. P., Eyring, V., Friedlingstein, P., Hurtt, G., ... Sanderson, B. M. (2016). The scenario model intercomparison project (scenariomip) for cmip6. *Geoscientific Model Development*, *9*(9), 3461–3482. doi: 10.5194/gmd-9-3461-2016

Pearson, K. (1894). Contributions to the mathematical theory of evolution. *Philosophical Transactions of the Royal Society of London. A*, *185*, 71–110. doi: 10.1098/rsta.1894.0003

Peel, D., & McLachlan, G. J. (2000). Robust mixture modelling using the t distribution. *Statistics and computing*, *10*(4), 339–348. doi: 10.1023/A:1008981510081

Phillips, J. G., Cane, M. A., & Rosenzweig, C. (1998). ENSO, seasonal rainfall pat-

terns and simulated maize yield variability in Zimbabwe. *Agricultural and Forest Meteorology*, *90*(1), 39–50. doi: 10.1016/S0168-1923(97)00095-6

Poveda, G., Jaramillo, A., Gil, M. M., Quiceno, N., & Mantilla, R. I. (2001). Seasonally in ENSO-related precipitation, river discharges, soil moisture, and vegetation index in Colombia. *Water Resources Research*, *37*(8), 2169–2178. doi: 10.1029/2000WR900395

Press, W. H., Teukolsky, S. A., Vetterling, W. T., & Flannery, B. P. (2007). *Numerical recipes 3rd edition: The art of scientific computing* (3rd ed.). Cambridge University Press. Retrieved from `http://www.amazon.com/Numerical-Recipes-3rd-Scientific-Computing/dp/0521880688/ref=sr_1_1?ie=UTF8&s=books&qid=1280322496&sr=8-1`

R Core Team. (2020). R: A language and environment for statistical computing [Computer software manual]. Vienna, Austria. Retrieved from `https://www.R-project.org/`

Rasmusson, E. M., & Carpenter, T. H. (1982). Variations in tropical sea surface temperature and surface wind fields associated with the Southern Oscillation/El Niño. *Monthly Weather Review*, *110*(5), 354–384. doi: 10.1175/1520-0493(1982)110⟨0354:VITSST⟩2.0.CO;2

Rayner, N. A., Parker, D. E., Horton, E. B., Folland, C. K., Alexander, L. V., Rowell, D. P., ... Kaplan, A. (2003). Global analyses of sea surface temperature, sea ice, and night marine air temperature since the late nineteenth century. *Journal of Geophysical Research: Atmospheres*, *108*(D14). doi: 10.1029/2002JD002670

Rayner, P. J., Enting, I. G., Francey, R. J., & Langenfelds, R. (1999). Reconstructing the recent carbon cycle from atmospheric CO_2, δ13C and O_2/N_2 observations. *Tellus B: Chemical and Physical Meteorology*, *51*(2), 213-232. doi: 10.3402/tellusb.v51i2.16273

Ren, H.-L., Lu, B., Wan, J., Tian, B., & Zhang, P. (2018). Identification standard for enso events and its application to climate monitoring and prediction in china. *Journal of Meteorological Research*, *32*(6), 923–936. doi: 10.1007/s13351-018-8078-6

Sanchez-Gomez, E., Somot, S., & Déqué, M. (2009). Ability of an ensemble of regional climate models to reproduce weather regimes over europe-atlantic during the period 1961–2000. *Climate Dynamics*, *33*(5), 723–736. doi: 10.1007/s00382-008-0502-7

Schwarz, G. (1978). Estimating the dimension of a model. *The annals of statistics*, *6*(2), 461–464. doi: 10.1214/aos/1176344136

Scrucca, L., & Raftery, A. E. (2015). Improved initialisation of model-based clustering using gaussian hierarchical partitions. *Advances in data analysis and classification*, *9*(4), 447–460. doi: 10.1007/s11634-015-0220-z

Seferian, R. (2018). *CNRM-CERFACS CNRM-ESM2-1 model output prepared for CMIP6 CMIP historical.* Earth System Grid Federation. Retrieved from `https://doi.org/10.22033/ESGF/CMIP6.4068` doi: 10.22033/ESGF/CMIP6.4068

Séférian, R., Nabat, P., Michou, M., Saint-Martin, D., Voldoire, A., Colin, J., ... Madec, G. (2019). Evaluation of CNRM Earth System Model, CNRM-ESM2-1: Role of Earth System Processes in Present-Day and Future Climate. *Journal of Advances in Modeling Earth Systems*, *11*(12), 4182-4227. doi: 10.1029/2019MS001791

Seland, Ø., Bentsen, M., Olivié, D., Toniazzo, T., Gjermundsen, A., Graff, L. S., ... Schulz, M. (2020). Overview of the Norwegian Earth System Model (NorESM2) and key climate response of CMIP6 DECK, historical, and scenario simulations. *Geoscientific Model Development*, *13*(12), 6165–6200. doi: 10.5194/gmd-13-6165-2020

Seland, Ø., Bentsen, M., Oliviè, D. J. L., Toniazzo, T., Gjermundsen, A., Graff,

L. S., ... Schulz, M. (2019). *NCC NorESM2-LM model output prepared for CMIP6 CMIP historical.* Earth System Grid Federation. Retrieved from https://doi.org/10.22033/ESGF/CMIP6.8036 doi: 10.22033/ESGF/CMIP6.8036

Sellar, A. A., Jones, C. G., Mulcahy, J. P., Tang, Y., Yool, A., Wiltshire, A., ... Zerroukat, M. (2019). UKESM1: Description and Evaluation of the U.K. Earth System Model. *Journal of Advances in Modeling Earth Systems*, *11*(12), 4513-4558. doi: 10.1029/2019MS001739

Swart, N. C., Cole, J. N., Kharin, V. V., Lazare, M., Scinocca, J. F., Gillett, N. P., ... Sigmond, M. (2019b). *CCCma CanESM5 model output prepared for CMIP6 CMIP historical.* Earth System Grid Federation. Retrieved from https://doi.org/10.22033/ESGF/CMIP6.3610 doi: 10.22033/ESGF/CMIP6.3610

Swart, N. C., Cole, J. N. S., Kharin, V. V., Lazare, M., Scinocca, J. F., Gillett, N. P., ... Winter, B. (2019a). The Canadian Earth System Model version 5 (CanESM5.0.3). *Geoscientific Model Development*, *12*(11), 4823–4873. doi: 10.5194/gmd-12-4823-2019

Takahashi, K., Montecinos, A., Goubanova, K., & Dewitte, B. (2011). Enso regimes: Reinterpreting the canonical and modoki el niño. *Geophysical Research Letters*, *38*(10). doi: https://doi.org/10.1029/2011GL047364

Takahashi, T., Sutherland, S. C., Wanninkhof, R., Sweeney, C., Feely, R. A., Chipman, D. W., ... de Baar, H. J. (2009). Climatological mean and decadal change in surface ocean pCO_2, and net sea-air CO_2 flux over the global oceans. *Deep Sea Research Part II: Topical Studies in Oceanography*, *56*(8), 554-577. doi: https://doi.org/10.1016/j.dsr2.2008.12.009

Tang, Y., Rumbold, S., Ellis, R., Kelley, D., Mulcahy, J., Sellar, A., ... Jones, C. (2019). *MOHC UKESM1.0-LL model output prepared for CMIP6 CMIP historical.* Earth System Grid Federation. Retrieved from https://doi.org/10.22033/ESGF/CMIP6.6113 doi: 10.22033/ESGF/CMIP6.6113

Taylor, K. E. (2001). Summarizing multiple aspects of model performance in a single diagram. *Journal of Geophysical Research: Atmospheres*, *106*(D7), 7183-7192. doi: 10.1029/2000JD900719

Thomas, E., Vimont, D., Newman, M., Penland, C., & Martínez-Villalobos, C. (2018). The role of stochastic forcing in generating ENSO diversity. *Journal of Climate*, *31*, 9125-9150. doi: 10.1175/JCLI-D-17-0582.1

Tjiputra, J. F., Schwinger, J., Bentsen, M., Morée, A. L., Gao, S., Bethke, I., ... Schulz, M. (2020). Ocean biogeochemistry in the Norwegian Earth System Model version 2 (NorESM2). *Geoscientific Model Development*, *13*(5), 2393–2431. doi: 10.5194/gmd-13-2393-2020

Trenberth, K. E., Branstator, G. W., Karoly, D., Kumar, A., Lau, N.-C., & Ropelewski, C. (1998). Progress during TOGA in understanding and modeling global teleconnections associated with tropical sea surface temperatures. *Journal of Geophysical Research: Oceans*, *103*(C7), 14291–14324. doi: 10.1029/97JC01444

Trenberth, K. E., & Stepaniak, D. P. (2001). Indices of el niño evolution. *Journal of Climate*, *14*(8), 1697 - 1701. doi: 10.1175/1520-0442(2001)014⟨1697:LIOENO⟩2.0.CO;2

Vaittinada Ayar, P., Bopp, L., Christian, J. R., Ilyina, T., Krasting, J. P., Séférian, R., ... Tjiputra, J. (2022). Contrasting projections of the enso-driven co_2 flux variability in the equatorial pacific under high-warming scenario. *Earth System Dynamics*, *13*(3), 1097–1118. Retrieved from https://esd.copernicus.org/articles/13/1097/2022/ doi: 10.5194/esd-13-1097-2022

Vautard, R. (1990). Multiple weather regimes over the north atlantic: Analysis of precursors and successors. *Monthly weather review*, *118*(10), 2056–2081. doi: 10.1175/1520-0493(1990)118⟨2056:MWROTN⟩2.0.CO;2

Vimont, D. J., Newman, M., Battisti, D. S., & Shin, S.-I. (2022). The Role of Seasonality and the ENSO Mode in Central and East Pacific ENSO Growth and Evolution. *Journal of Climate*, *35*(11), 3195–3209. doi: 10.1175/JCLI-D-21-0599.1

Vimont, D. J., Wallace, J. M., & Battisti, D. S. (2003). The Seasonal Footprinting Mechanism in the Pacific: Implications for ENSO. *Journal of Climate*, *16*(16), 2668–2675. doi: 10.1175/1520-0442(2003)016⟨2668:TSFMIT⟩2.0.CO;2

Vrac, M., Vaittinada Ayar, P., & Yiou, P. (2014). Trends and variability of seasonal weather regimes. *International Journal of Climatology*, *34*(2), 472–480. Retrieved from `http://dx.doi.org/10.1002/joc.3700` doi: 10.1002/joc.3700

Vrac, M., & Yiou, P. (2010). Weather regimes designed for local precipitation modeling: Application to the Mediterranean basin. *J. Geophys. Res.*, *115, D12103*. doi: 10.1029/2009JD012871

Wieners, K.-H., Giorgetta, M., Jungclaus, J., Reick, C., Esch, M., Bittner, M., ... Roeckner, E. (2019). *MPI-M MPI-ESM1.2-LR model output prepared for CMIP6 CMIP historical.* Earth System Grid Federation. Retrieved from `https://doi.org/10.22033/ESGF/CMIP6.6595` doi: 10.22033/ESGF/CMIP6.6595

Yiou, P., & Nogaj, M. (2004). Extreme climatic events and weather regimes over the North Atlantic: When and where? *Geophys. Res. Lett.*, *31*, L07202. doi: 10.1029/2003GL019119

Yukimoto, S., Kawai, H., Koshiro, T., OSHIMA, N., YOSHIDA, K., URAKAWA, S., ... ISHII, M. (2019). The Meteorological Research Institute Earth System Model Version 2.0, MRI-ESM2.0: Description and Basic Evaluation of the Physical Component. *Journal of the Meteorological Society of Japan*, *97*(5), 931-965. doi: 10.2151/jmsj.2019-051

Yukimoto, S., Koshiro, T., Kawai, H., Oshima, N., Yoshida, K., Urakawa, S., ... Adachi, Y. (2019). *MRI MRI-ESM2.0 model output prepared for CMIP6 CMIP historical.* Earth System Grid Federation. Retrieved from `https://doi.org/10.22033/ESGF/CMIP6.6842` doi: 10.22033/ESGF/CMIP6.6842

Zebiak, S. E., & Cane, M. A. (1987). A model El-Niño Southern Oscillation. *Monthly Weather Review*, *115*, 2262-2278. doi: 10.1175/1520-0493(1987)115⟨2262:AMENO⟩2.0.CO;2

Zhang, Y., Wallace, J. M., & Battisti, D. S. (1997). ENSO-like interdecadal variability: 1900-93. *Journal of Climate*, *10*, 1004-1020. doi: 10.1175/1520-0442(1997)010%3C1004:ELIV%3E2.0.CO;2%7D

Ziehn, T., Chamberlain, M., Lenton, A., Law, R., Bodman, R., Dix, M., ... Druken, K. (2019). *CSIRO ACCESS-ESM1.5 model output prepared for CMIP6 CMIP historical.* Earth System Grid Federation. Retrieved from `https://doi.org/10.22033/ESGF/CMIP6.4272` doi: 10.22033/ESGF/CMIP6.4272